

Sputtering of indium using Au_m projectiles: Transition from linear cascade to spike regime

A. V. Samartsev, A. Duvenbeck, and A. Wucher

Department of Physics, University of Duisburg—Essen, 47048 Duisburg, Germany

(Received 1 February 2005; revised manuscript received 21 April 2005; published 14 September 2005)

We have investigated the yields and emission velocity distributions of neutral In atoms and In_2 dimers sputtered from a pure indium surface under bombardment with $Au_m^+(m=1, 2, 3)$ projectile ions. It is shown that 5-keV Au_1 bombardment leads to results in full compliance with linear cascade sputtering theory. All polyatomic projectiles are found to generate an additional low-energy contribution to the sputtered flux, which increases with increasing projectile nuclearity and energy and completely dominates the spectra under 10-keV Au_3 bombardment. Analysis shows that this contribution cannot be explained in terms of thermal spike sputtering models. Instead, the results indicate a spike emission mechanism, which closely resembles a free expansion of a supercritically heated subsurface volume.

DOI: [10.1103/PhysRevB.72.115417](https://doi.org/10.1103/PhysRevB.72.115417)

PACS number(s): 79.20.Rf, 82.30.Nr

I. INTRODUCTION

If a solid is bombarded with keV ions, particles are released from the surface due to a cascade of mostly elastic collisions, a process which is generally termed “sputtering.” The flux of sputtered particles contains atomic as well as molecular species in different charge and excitation states and is in most cases strongly dominated by neutral target atoms. Under bombardment with monoatomic projectiles, the physics underlying the emission process appear to be reasonably well understood.¹ In particular, the velocity or kinetic energy distributions of the emitted particles are found to carry a characteristic signature of the sputtering process. For most projectile-target combinations, the dynamics are generally described as a linear collision cascade modeled by analytical transport theory,^{2,3} resulting in a strongly nonthermal emission energy distribution,^{3,4} which has been verified both experimentally (see Ref. 5 for a review) and by computer simulations.⁶

Already early on, however, it has been discovered that deviations from this linear cascade behavior can be observed when projectiles containing more than one atom are used instead of monoatomic projectile species (see Ref. 7 for a fairly recent review). These effects were first observed to manifest as a nonlinear yield enhancement,^{8–12} i.e., the total sputter yield (average number of sputtered atoms per impinging projectile) measured under cluster impact exceeds the sum of the yields generated by the individual projectile atoms impinging with the same velocity. The prevailing qualitative interpretation of this observation is that the projectile disintegrates upon impact, and the collision cascades initiated by the individual constituent atoms overlap to form a dense collisional spike, which does not satisfy the linearity condition (low density of moving atoms) any more.⁷

More recent work involving gold cluster projectiles containing up to 13 atoms^{13,14} revealed very large yield enhancement effects, which appear to scale with the projectile nuclearity. These results are often interpreted in terms of analytical models describing particle emission to originate from the superposition of a linear cascade contribution—ejected during the early stages of a collision cascade—and a spike contribution developing at later times.^{15–19} In that sense, the

definition of a spike means the spatial region in which a very dense collision cascade is propagating. In many of the published spike theories, particle emission is treated as thermal evaporation from such a region, which is then termed a “thermal spike.”^{16,18}

So far, only few experiments have been conducted where the emission energy spectra of sputtered species were measured under polyatomic projectile impact. Moreover, many of the existing data were taken for secondary ions, where it is not clear whether the observed energy spectra are influenced by an emission velocity-dependent ionization mechanism. Corresponding data for sputtered *neutral* species are restricted to only a few publications. Oostra *et al.*²⁰ measured the energy distributions of Au atoms sputtered from a gold surface under bombardment with 8-keV I_2^+ and 4-keV I^+ projectiles and used the acquired data to identify a growing spike contribution to the sputter yield under diatomic ion bombardment. These experiments are quite similar to those performed here, but we will show that the results appear to be questionable. Wang *et al.*²¹ measured the energy distributions of sputtered Cu atoms under bombardment with 3.6-keV N_2^+ , CF_2^+ , and CF_3^+ ions in comparison with those produced by Ar^+ and N^+ projectiles of the same impact energy. From our recent findings for 10-keV SF_m^+ bombardment of metal surfaces,²² we conclude that for these light projectiles the studied impact energy is too low to observe any sizeable nonlinear enhancement effect.

Therefore, one must conclude that reliable information regarding the influence of nonlinear spike contributions on the emission energy distribution of sputtered neutral particles ejected under polyatomic projectile impact is still lacking. In the present work, we use gold cluster ions Au_m^+ with $m = 1, \dots, 3$ and impact energies of 5 and 10 keV to bombard a clean, polycrystalline indium surface. We present measurements of the total sputtering yields and the kinetic energy spectra of neutral In atoms and In_2 dimers emitted along the surface normal. The resulting spectra are compared with the prediction of linear cascade sputtering theory. Results show that strong nonlinear yield enhancements are observed which originate from additional spike contributions producing predominantly low-energy emission. Comparisons of measured

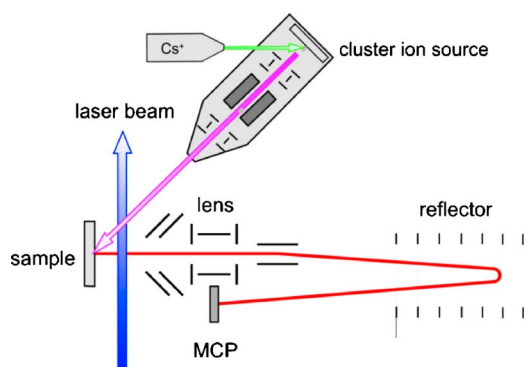


FIG. 1. (Color online) Schematic setup of the experimental arrangement used for TOF mass spectrometric detection of sputtered neutral atoms and clusters.

energy spectra with published theoretical emission models reveal that evaporation from a thermal spike cannot explain the data. Instead, the results constitute strong evidence for a quasifree expansion of an overcritically heated subsurface volume with complete disruption of the surface.

II. EXPERIMENTAL

The experimental setup used for mass and energy spectrometric detection of sputtered neutral particles is sketched in Fig. 1. The system consists of an ion source generating cluster ions of a desired element and a laser-photoionization time-of-flight (TOF) mass spectrometer used to detect the neutral species sputtered from the sample surface under bombardment with these projectiles. All components of the setup are housed in an ultrahigh vacuum chamber with a base pressure of about 10^{-9} mbar rising to several 10^{-8} mbar during operation of the ion source.

The newly developed sputter ion source generating the projectile ions is described in detail elsewhere.²³ The working principle is based on the production of negative secondary ions from a negatively biased, selectable target surface (here gold) bombarded by positive cesium ions of 10 keV. The generated atomic and polyatomic ions are extracted by a high-voltage (HV) immersion lens, mass separated by a Wien filter and focused onto the sample surface (here indium). The electric field in the Wien filter is employed to chop the ion beam with selectable pulse lengths ranging from 100 ns to infinity. In the present work, Au^- , Au_2^- , and Au_3^- projectile ions of 5 and 10 keV impact energy have been used with beam currents around 200 nA (Au^-) and 10 nA (Au_2^- and Au_3^-), respectively. The projectiles impinge onto a polycrystalline indium surface under an angle of 45° with respect to the surface normal.

The method and procedures used to obtain TOF mass spectra and kinetic energy distributions of sputtered neutral particles have been described in much detail elsewhere²⁴ and will be, therefore, described here only briefly. Neutral particles emerging from the sample surface are photoionized by single-photon absorption from an intense, pulsed UV laser operated at a wavelength of 193 nm (photon energy 6.4 eV) with pulse energies up to 150 mJ and a temporal pulse dura-

tion of about 20 ns. The laser beam is shaped to a cross section of about 1 mm^2 and steered parallel to the sample surface at the closest possible distance of about 0.5 mm. Under these conditions, maximum peak power densities around 10^8 W/cm^2 are obtained in the ionization volume. As demonstrated elsewhere,²⁵ this value is large enough to drive the photoionization process into saturation. The laser intensity can be varied over several orders of magnitude by a set of rotatable dielectric attenuators.

The ionization laser is fired at a selectable time delay after the end of the projectile ion pulse. During ion bombardment and laser pulse, the sample is kept at a small negative potential of -300 V with respect to the ground, in order to suppress a background signal arising from positive secondary ions. Negative secondary ions, on the other hand, are accelerated by that potential to drift energies which prevent them from being reflected in the TOF spectrometer. Shortly ($\sim 100 \text{ ns}$) after the laser pulse, a HV pulse of $+1400 \text{ V}$ is applied to the sample in order to sweep the generated photoions into the TOF spectrometer. During acquisition of energy integrated mass spectra, a relatively long primary ion pulse of several microseconds duration is selected in order to ensure that the ionization volume is filled with particles of all relevant emission velocities.

To determine the emission velocity distribution of sputtered neutral particles, the projectile pulse duration is reduced to 200 ns. In addition, the laser beam is positioned at a distance of 2 mm in front of the surface and focused to a cross section of about $0.3 \times 0.5 \text{ mm}^2$ [full width at half maximum (FWHM)] with the short dimension along the surface normal. Moreover, the laser intensity is attenuated to a peak power density of about $2 \times 10^6 \text{ W/cm}^2$ in order to avoid saturation of the photoionization process (see below). The emission velocity of the detected neutral particles is then selected via their flight time from the sample surface to the ionization volume by a controlled variation of the time delay t_d between the projectile ion pulse and the laser pulse. The accurate calibration of the velocity $v = r/t_d$ requires precise knowledge of the distance r between the laser and the surface, which is measured by translating the laser beam to the surface and monitoring the TOF signal generated by laser ablation once the laser beam hits the sample.

The zero of the delay time t_d is critical since it depends on the flight time of the projectile ions from the Wien filter to the sample surface as well as the firing delay of the ionization laser. Both quantities depend on the exact experimental conditions and, therefore, must be individually compensated in every experiment. This was done by translating a microchannel plate (MCP) detector into the sample position in order to monitor the projectile ion and laser pulses. An example of such a measurement is depicted in Fig. 2. The recorded MCP signal track shows the peak generated by the projectile ion impact along with a second peak generated by the UV laser stray light. The oscillatory structure, which is visible shortly after the laser pulse, arises from rf noise generated by the fast HV switch pulsing the extraction field. The acquisition of data like that presented in Fig. 2, therefore, allows a complete calibration of the relevant timing. The velocity resolution in these experiments is determined by the temporal duration of the projectile ion pulse, the duration of

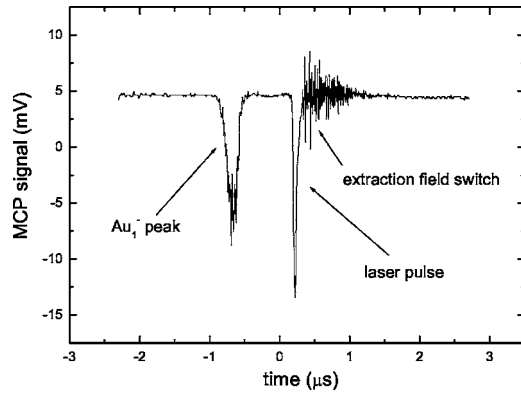


FIG. 2. Monitor signal measured on a second MCP detector mounted in place of the sample surface for the relative timing calibration of projectile impact, ionizing laser, and pulsed ion extraction field.

the laser pulse, and the spatial extension of the laser beam or ionization volume in the direction along the surface normal. Under the present experimental conditions, it is estimated as $\Delta v/v \approx 1.5 \times 10^{-1} \{1 + 0.067 \times v(\text{km/s})\}$.

The time dispersed (mass separated) photoions are detected by a dual MCP assembly in a chevron arrangement. The front electrode of the detector is held at -2000 V with respect to the ground, resulting in a total ion impact energy of 3.4 keV. As shown previously,²⁵ this energy is sufficient to detect indium clusters containing up to about 30 atoms without significant size discrimination effects. The output current delivered by the detector is directly digitized using a fast transient recorder. In order to avoid detector saturation, the gain voltage across the MCP is reduced such as to ensure that the maximum recorded signal did not exceed a height of about 100 mV at 50Ω termination. All recorded spectra are averaged over 200 projectile ion pulses for noise reduction.

III. RESULTS AND DISCUSSION

The main goal of the present work is to enlighten the fundamental mechanisms of nonlinear particle ejection from a metallic surface under bombardment with heavy polyatomic projectiles. In order to estimate the relative role of nonlinear processes, we first determine the variation of the total sputtering yield as a function of the nuclearity (i.e., the number m of constituent atoms) of the projectile by the integration of the measured TOF mass spectra. Following the route of a previous work, nonlinear “spike” contributions are identified as a relative enhancement of the yield measured for an Au_m projectile versus m times that produced by Au projectiles of the same impact velocity (Sec. III A). As a second step, we then investigate the dependence of the emission energy or velocity spectrum of sputtered neutral indium atoms and dimers on the projectile nuclearity. The combination of both types of information allows us to assign a characteristic velocity spectrum to that part of the sputtered material which is emitted from a spike (Sec. III B). These results are then compared with prevailing spike models in

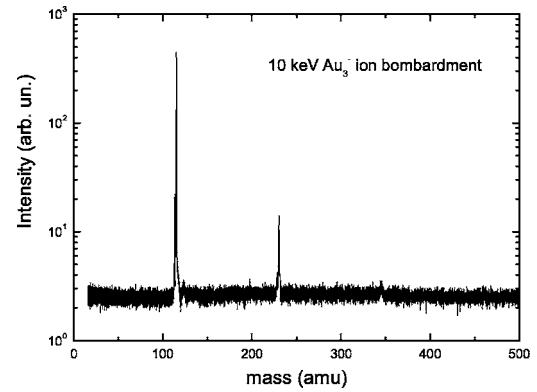


FIG. 3. TOF mass spectrum of neutral atoms and clusters sputtered from a pure, polycrystalline indium surface under bombardment with 10-keV Au_3^- ions impinging under 45° with respect to the surface normal. The ionizing laser was operated at a wavelength of 193 nm and a power density of about 10^8 W/cm².

order to draw important conclusions regarding the emission mechanism under nonlinear spike conditions (Sec. III C).

A. Total sputter yield

Figure 3 shows a mass spectrum of neutral atoms and clusters that are sputtered from a clean polycrystalline indium foil. The spectrum was recorded under bombardment with 10-keV Au_3^- ions impinging under 45° with respect to the surface normal, using 193-nm UV laser radiation with a peak power density around 10^8 W/cm² for postionization. As shown in detail elsewhere, this laser intensity ensures complete saturation of the postionization process, and the recorded signal, therefore, can be taken as representative for the number density of the respective particles in the ionization volume. The mass spectrometer is operated at a resolution of about $m/\Delta m = 250$, which appears to be approximately constant across the whole spectrum.

Two groups of peaks are identified which correspond to In atoms and In_2 dimers with the expected isotopic abundance patterns. Apart from a very small signal corresponding to In_3 , the spectrum does not contain any other significant peaks, indicating that the sample is clean and free of a possible gold contamination from the projectiles. In agreement with our earlier data using atomic projectiles,²⁵ all larger In_n clusters exhibit signals at least one order of magnitude smaller than that of the dimers. This finding demonstrates that—also under the cluster bombardment conditions employed to acquire the data of Fig. 3, which lead to strong nonlinear sputtering (see below)—indium clusters contribute only negligibly to the total sputtered flux. Hence, we take the integrated monomer signal—normalized to the respective projectile ion current—as representative of the total sputtering yield under the prevailing bombardment conditions.

At first sight, this assumption appears to be at variance with the conjecture of Rehn *et al.*^{26–28} who concluded that in the nonlinear regime a sizeable fraction of the total sputter yield is contributed by the emission of mesoscopic clusters. To discuss this apparent discrepancy, we note that the work of Refs. 26–28 has been performed under very different ex-

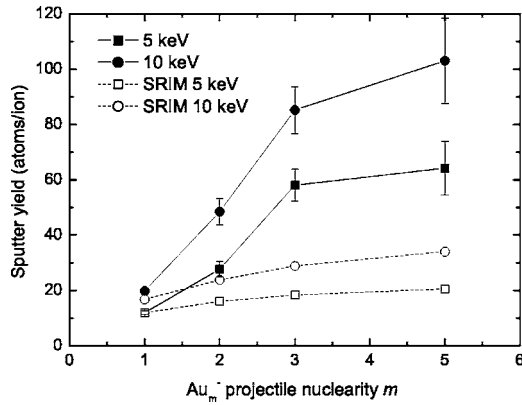


FIG. 4. Total sputter yield vs nuclearity m of Au_m projectiles impinging with kinetic energies of 5 and 10 keV onto a polycrystalline indium surface. Open symbols: linear cascade prediction from SRIM2003 computer simulations.

perimental conditions (transmission sputtering at much higher impact energies) than employed here. Moreover, our previous data²⁵ show that for indium, as the bombarded target material, the n^{-2} yield distribution measured for larger sputtered clusters cannot be extrapolated toward small clusters or even monomers.

The resulting yield variation as a function of the projectile nuclearity is depicted in Fig. 4. Since our TOF spectrometer is not calibrated in terms of absolute collection efficiency, only relative yield ratios can be extracted from the measured mass spectra. In order to arrive at absolute values on the ordinate axis, the data have been normalized to that measured for impact of 5-keV Au projectiles and multiplied with a theoretical sputter yield calculated for these bombardment conditions by means of the binary collision Monte-Carlo computer simulation program SRIM2003.²⁹ The resulting value of about 12 atoms/ion compares well with that calculated from analytic sputtering theory [~ 15 atoms/ion (Ref. 30)]. The basis underlying this procedure is that for 5-keV Au bombardment the sputtering process is assumed to be dominated by linear cascades. As shown below, this assumption is realistic. The theoretical estimate was used since no experimental literature data appear to exist for the gold-indium projectile-target combination. Note that the normalization only influences the absolute yield values and, in particular, does not alter the measured relative yield variation.

At first sight, it is obvious that the polyatomic nature of the projectile leads to a yield increase with respect to the isoenergetic monoatomic projectile. It is important to note at this point that—due to the fact that our experiments are done under conditions of constant impact energy E_B of all projectiles—this observation alone constitutes *no* indication of a nonlinear enhancement effect. In order to illustrate that point, we have simulated the linear yield generated by an Au_m projectile as the sum of those expected for impact of the constituent atoms independently. The latter was again calculated using the SRIM2003 program for impact of Au projectiles onto indium at a kinetic energy of E_B/m . The resulting yield values have been included in Fig. 4 as open symbols. In the discussion of these data, it is important to note that the physical concept behind the Monte-Carlo SRIM code treats the

TABLE I. Nonlinear yield enhancement factor, i.e., ratio between measured sputter yield and that predicted by linear cascade theory, for nuclearity m and impact energy of Au_m projectiles.

m	5 keV	10 keV
1	1.00	1.18
2	1.73	2.03
3	3.17	2.96
5	3.13	3.03

collision cascade as a sequence of binary collisions between a moving atom and a target atom initially at rest. As pointed out by Andersen in his extensive review of the topic,⁷ this is exactly the definition of a linear collision cascade. In the limit of the validity of the binary collision approximation, the resulting values, therefore, can be regarded as representative of the yield contribution expected from linear cascade theory. Since the kinetic impact energies applied here are significantly below that at which the maximum nuclear stopping power is reached (~ 550 keV for the Au \rightarrow In system), also the linear cascade model predicts a yield increase with increasing projectile nuclearity, which is, however, much less pronounced than that observed in our experimental data. Therefore, we take the difference between closed and open symbols in Fig. 4 as the nonlinear yield contribution, which is found to outweigh the linear part as soon as the projectile contains more than two atoms. Calculating the ratio between both values, we determine the nonlinear yield enhancement factors compiled in Table I. Note that the particular value depicted for 10-keV Au_2 impact is determined exclusively from experimental data in the same way as is done in Refs. 8 and 10–12 and, therefore, is independent of the accuracy of the computer simulation.

While it is clear that all polyatomic projectiles produce nonlinear yield enhancement, the data presented in Fig. 4 and Table I also reveal such effects even for the monoatomic projectiles impinging with 10 keV. The latter finding is not surprising; in fact, it is in agreement with many earlier sputtering studies where nonlinear yield enhancements were generally found for impact of heavy atomic projectiles with large kinetic energies (cf. Refs. 31–33 for reviews). The general conjecture emerging from the available experimental yield data is that nonlinear effects should occur whenever the total sputter yield exceeds values around 20.³² As seen from the data in Fig. 4 and the discussion in the following section, our results appear to be in very good agreement with that statement.

B. Energy distributions

As explained in Sec. II, the emission velocity or energy spectra are determined by a controlled variation of the delay time t_d between the projectile ion pulse and the ionizing laser pulse. In order to convert the resulting flight time distributions into kinetic energy spectra, it is important to note that the laser postionization experiment generally detects the superposition of two signal contributions: while the first (“number density”) part represents those sputtered neutral

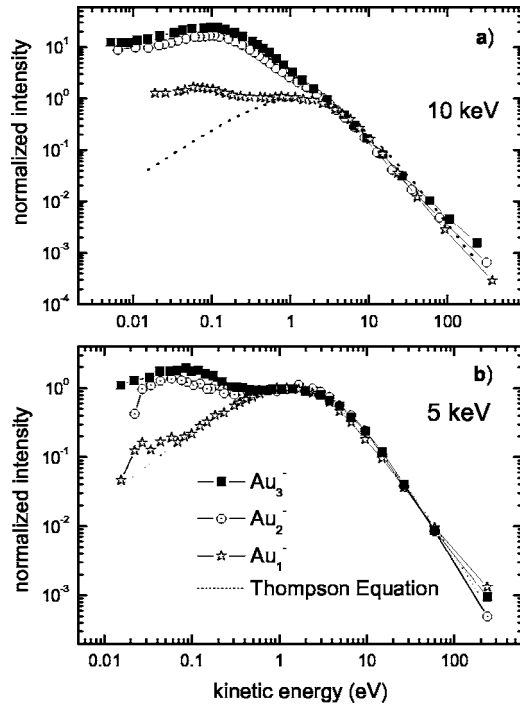


FIG. 5. Emission energy spectra of neutral In atoms sputtered from a polycrystalline indium surface under impact of (a) 10-keV and (b) 5-keV Au_m⁻ projectile ions. Dotted line: prediction from linear cascade theory.

particles which reside in the ionization volume *at* the firing time of the ionization laser, the second (“flux”) contribution arises from those particles which enter the ionization volume and get ionized *during* the laser pulse. Apart from the trivial conversion from flight time to emission velocity or energy, this leads to a Jacobian conversion of the measured signal $S(t_d)$ according to

$$f(v) \propto \frac{S(t_d) \times t_d}{\Delta r + v \Delta t} \quad \text{or} \quad f(E) \propto \frac{S(t_d) \times t_d^2}{\Delta r + v \Delta t}. \quad (1)$$

Here, Δr denotes the spatial extension of the ionization volume along the surface normal and Δt is the laser pulse duration. A detailed analysis³⁴ shows that the second term in the denominator of Eq. (1)—arising from the flux contribution—only needs to be taken into account if the postionization efficiency is driven far into saturation. Therefore, the ionization laser was strongly attenuated in these experiments and this term can safely be neglected here.

The resulting kinetic energy spectra of neutral In atoms ejected along the surface normal under bombardment with different projectiles are displayed in Fig. 5. These data can now be compared with the distribution expected from linear cascade theory⁴

$$f(E) \propto \frac{E}{(E + U_0)^3}, \quad (2)$$

where U_0 denotes the surface binding energy of the ejected atoms. In principle, minor corrections to the exponent in the denominator have been proposed,³ which are neglected here.

Although not rigorously justified, the surface binding energy is often approximated as the thermodynamic sublimation energy of the target material. Taking U_0 as a fit parameter, we obtain the best fit for $U_0 = 2.3$ eV slightly below the respective value of 2.6 eV for indium. The resulting curve, normalized to the maximum of the 5-keV Au₁⁻ data, is indicated by the dotted line. It is apparent that the linear cascade prediction is in almost perfect agreement with the energy distribution measured for impact of 5-keV Au⁻ projectiles. This finding provides strong evidence for our earlier assumption of a linear collision cascade for this projectile and impact energy. If the projectile nuclearity is increased under conditions of constant impact energy, deviations from the linear cascade distribution are found which manifest as an additional contribution at low emission energies. Switching to higher impact energy, Fig. 5(a) shows that such a contribution is already observed for the monoatomic projectile. It is found to strongly increase and completely dominate the measured spectra for polyatomic projectiles.

In combination with the yield data presented in the preceding section, we, therefore, conclude that the nonlinear “spike” contribution of the measured yield arises predominantly from low energy particles. Qualitatively, this observation is in agreement with the results of earlier energy distribution measurements performed under the impact of heavy and high-energy monoatomic and, in some cases, polyatomic projectiles.⁷ As discussed in Andersen’s review,⁷ it is also not surprising since the breakdown of the linearity condition in the cascade is expected to occur at low kinetic energies. In any way, the data depicted in Fig. 5 presents clear evidence that the collision cascade initiated by the impact of heavy polyatomic projectiles onto a metallic surface is completely dominated by a dense collisional spike which shows no resemblance with a linear cascade any more.

In order to quantitatively test the above conjecture, we isolate the spike contribution from the measured energy spectra by subtracting the linear cascade part. This is possible since the distributions appear to be dominated by the linear cascade contribution in the high-energy regime. The normalization of the data presented in Fig. 5 was accordingly chosen such that the high-energy tails of the different energy spectra coincide. The pure spike contribution is then extracted by subtraction of either the theoretical linear cascade fit curve or the 5-keV Au₁⁻ data. The resulting energy distributions are displayed in Fig. 6. According to the above discussion, we suppose these spectra to represent the emission energy distribution of atoms ejected by a spike mechanism effective during the later stage of the collision cascade. Integration of the data presented in Fig. 6 and comparison with the integral of the total spectra shown in Fig. 5, therefore, should directly correspond to the nonlinear yield enhancement presented in Table I. We examine that conjecture for 10-keV Au₂⁻ projectiles, since this is the only case where the nonlinear yield enhancement can be identified from the experimental data alone (i.e., without the uncertainty of the SRIM simulation). From the integration of the respective energy spectra, we obtain an enhancement factor of 1.96, which is in almost perfect agreement with the value of 2.03 determined from the yield data.

Looking at Fig. 6, a striking observation is that all spike-related emission energy distributions peak at very low ener-

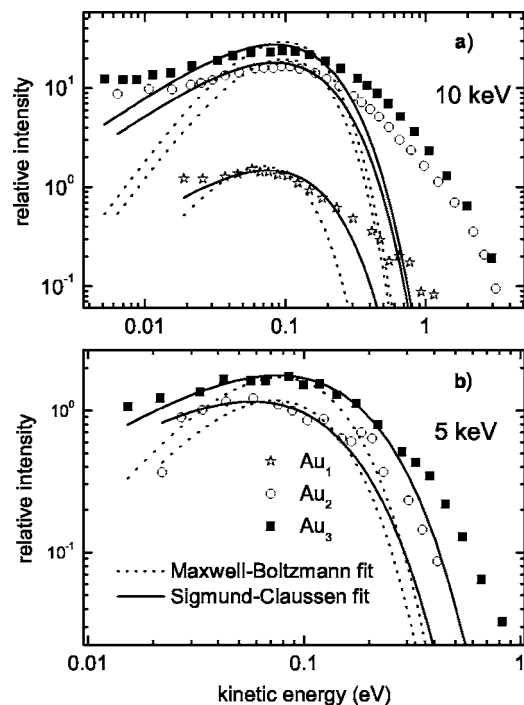


FIG. 6. Spike contribution of kinetic emission energy spectra of neutral In atoms sputtered from a polycrystalline indium surface under impact of (a) 10-keV and (b) 5-keV Au_m^- projectiles. Dotted lines: least-squares fit of a *Maxwell-Boltzmann* distribution [Eq. (3)]. Solid lines: least-squares fit of *Sigmund-Claussen* (Ref. 16) thermal spike model.

gies of 0.1 eV or below. This is also true for monoatomic Au_1^- projectiles, a finding which appears to agree with early work by Thompson and Nelson.³⁵ It is, however, at variance with a body of similar data published later,^{20,21,36–38} where much larger peak energies were generally found. In particular, we note that the energy distributions of sputtered Au atoms measured in Ref. 20 for impact of 4-keV I^+ and 8-keV I_2^+ projectiles exhibit maxima at energies of several eV, which have been attributed to an apparent spike contribution. A possible reason for this discrepancy is given by the fact that the work of Refs. 20 and 37–39 was performed using a time-of-flight method in combination with electron-impact postionization of sputtered neutral particles. From our own experience with this technique,⁴⁰ we know that this method leads to a principally unavoidable discrimination of low-energy particles due to ion trapping in the space charge generated by the electron beam. Since this effect is absent in photoionization, we conclude that velocity distributions taken with the laser-postionization method employed here must be more reliable at low energies. Comparing our spectra to those obtained in Ref. 21, we note that these data have been acquired using a nonresonant *multiphoton* postionization (MPI) scheme as opposed to single-photon ionization (SPI) employed here. The fundamental difference between both methods is that the cross section for truly nonresonant MPI of atoms is generally much lower than that for dissociative ionization of molecules; therefore, the measured atom signals are often superimposed by those arising from sputtered clusters. It has been demonstrated⁴¹ that this fact may

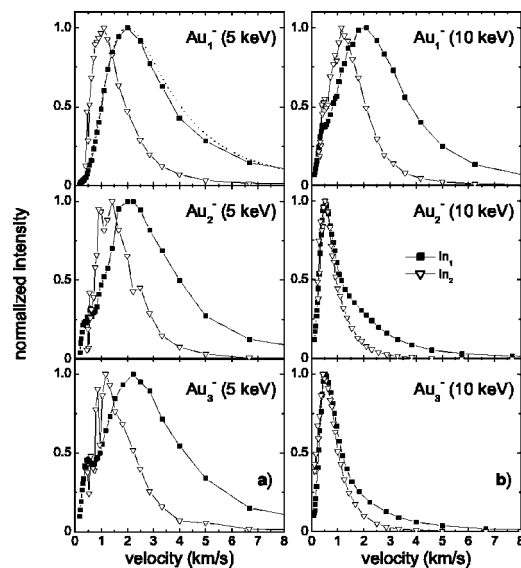


FIG. 7. Emission velocity spectra of neutral In atoms and In_2 dimers sputtered from a polycrystalline indium surface under bombardment with (a) 5-keV Au_1^- and (b) 10-keV Au_3^- projectile ions. Dotted line: linear cascade theory [Eq. (2)] with $U_0=2.3$ eV.

lead to the acquisition of erroneous emission velocity distributions of sputtered atoms. As pointed out a number of times in the literature,^{24,41} this problem is greatly reduced in SPI postionization experiments since the related cross sections of atoms and clusters are similar. Therefore, we conclude that the data presented here constitute the most reliable information on the energy distributions of atoms sputtered from a collisional spike available to date. From Fig. 6, it is apparent that the average emission energy of atoms is much lower than the sublimation energy of the sample material. The implication of this finding will be discussed below.

So far, only the atomic species among the flux of sputtered particles have been considered. As it turns out, another interesting piece of information on the sputtering mechanism is gained by comparing the emission velocity spectra of ejected monomers and clusters. As an example, corresponding data measured for sputtered neutral In_2 dimers are plotted in Fig. 7 along with those of the monomers. Under 5-keV Au_1^- bombardment, a dimer spectrum is produced which peaks at lower emission velocity and falls off more steeply toward high velocities than that of the monomers. This result is in accordance with practically all results of similar studies conducted in the past^{24,25,42–46} as well as with simple analytical models of dimer formation in sputtering.^{47–49} Therefore, it represents another manifestation that this case clearly falls into the linear collision cascade regime of sputtering. Upon transition to polyatomic projectiles and higher impact energies, a growing low-velocity component is observed for both sputtered species, until for 10-keV Au_2^- and Au_3^- impact, the case of a spike-dominated emission process is reached. The corresponding data in Fig. 7 reveal a striking change of the measured spectra in such a way that now the sputtered monomers and dimers exhibit a practically *identical* velocity distribution. Translated to emission energy, this means that now the dimer spectrum peaks at *higher* kinetic energies than

that of the monomers. The relevance of this observation will be discussed in Sec. III C.

C. Comparison with theoretical spike models

The energy spectra depicted in Fig. 6 are now compared to predictions from published spike sputtering models, a review of which can be found in Ref. 50. We first examine the thermal spike approach, which has been cast in a variety of different formulations. In its simplest form, the velocity spectrum of atoms emitted by thermal evaporation from a locally heated surface is predicted as a Maxwell-Boltzmann distribution according to

$$f(E) \propto E \exp\left[-\frac{E}{kT}\right]. \quad (3)$$

Corresponding fits have been made to some of the cited experiments and were claimed to agree quite well.^{37,38} If we fit Eq. (3) to the data presented in Fig. 6, we obtain the results included as dotted lines. It is immediately evident that the measured spectra cannot be explained by such a model, since the Maxwell-Boltzmann distribution severely underestimates the data in the energy regime above 0.3 eV. As pointed out in Ref. 16, this finding is not surprising due to the strong temporal and spatial variation of the spike temperature, leading to a significantly modified energy spectrum as compared to Eq. (3). Least-squares fits of the more sophisticated distribution predicted, for instance, by the Sigmund-Claussen model¹⁶ are, therefore, also included in Fig. 6 as solid lines. Although the results fit the experimental data slightly better than Eq. (3), it is evident that also this functional dependence is not capable of describing the measured distributions, in particular for higher impact energy. The problem with thermal spike models becomes even more evident if the extracted fitting parameters are used to estimate the relative magnitude of the nonlinear yield contribution. As is already evident from the observed most-probable emission energies (~ 0.1 eV), the initial spike core temperature value obtained from the energy distribution measurement is of the order of 1000 K. Inserting that value into the respective yield formulae of Ref. 16, the model predicts a ratio between the thermal spike and linear cascade yield contributions $Y_{th}/Y_{lin} \sim 10^{-11}$, which is by many orders of magnitude at variance with the measured data depicted in Table I. As a consequence, one has to conclude that the experimental data obtained here cannot be consistently interpreted in terms of a thermal evaporation mechanism.

Another piece of evidence against thermal spikes is given by the data presented in Fig. 7. If particle emission would be governed by thermal evaporation, one would expect identical emission energy distributions of all species leaving the surface, which is clearly not the case. Instead, we observe similar emission velocity distributions for sputtered monomers and clusters under spike conditions. This finding reminds one of the situation in a nozzle expansion, as is often employed for the generation of cluster beams.⁵¹ In fact, molecular dynamics studies^{19,52–56} have revealed that concepts of fluid dynamics rather than thermal evaporation from a heated surface must be employed in the description of the sputtering

process under strongly nonlinear spike conditions. Based on that observation, several analytical models taking up that picture have been proposed.^{19,57} They show that the emission process can be understood as a quasifree expansion of a sub-surface sample volume which has been heated to temperatures above the critical point and, hence, become gasified in the course of the collision cascade. Since the density is still close to that of the solid, immense pressure builds up which leads to a complete disruption of the surface, typically followed by the formation of a crater. In order to emphasize the distinction to an ordinary thermal evaporation mechanism, Averback and Ghaly⁵⁴ as well as Jakas *et al.*⁵⁷ have described such a scenario as a “microexplosion.” As demonstrated in Ref. 57, the resulting emission velocity field resembles that of a point source located slightly below the surface, leading to relatively broad emission angle distributions as observed experimentally by Andersen *et al.*⁵⁸ In a way, the process implies a significant reduction of the effective surface binding energy of the emitted particles and does in that sense agree with an idea put forward by Thompson *et al.*³¹ In principle, such a scenario should develop under conditions where the energy density in the collision cascade greatly exceeds the sublimation energy per atom. For rare gas targets, due to the low sublimation energy, this situation is already achieved under low-energy impact of rare gas atoms. For metallic targets, a similar situation is apparently realized under heavy polyatomic projectile impact.

Unfortunately, most of the published spike models concentrate on a description of the sputter yield and do not make an explicit prediction of the emission velocity or energy distribution. A notable exception is the “gas flow” model of Urbassek and Michl,¹⁹ which predicts the emission energy spectrum of sputtered atoms as^{19,52}

$$f(E) \propto \frac{1}{\sqrt{\pi} \times \varepsilon \times \varepsilon^* \times \varepsilon} \left[\gamma\left(\frac{5}{2}, \varepsilon \times (1 + t_c/t_0)\right) - \gamma\left(\frac{5}{2}, \varepsilon\right) \right], \quad (4)$$

Here, $\varepsilon = E/kT$ is the reduced energy and γ denotes the incomplete Gamma function. The reduced critical energy

$$\varepsilon^* = \frac{M(l/t_0)^2}{2kT_0} \quad (5)$$

corresponds to a particle of mass M moving with critical speed $v^* = l/t_0$, i.e., traveling the cascade depth l within the “quenching time” t_0 . The physical meaning of t_0 is a time constant describing the dissipation of energy out of the cascade volume into the bulk of the crystal by a power law decay term $(1 + t/t_0)^{-v}$ with $v=1$ for cylindrical symmetry.¹⁹ The quantity $1 + t_c/t_0 = (T_0/T_{con})^{1/v}$ approximately determines the time t_c at which freezing (recondensation) starts. Here T_0 is the initial temperature of the energized volume and T_{con} is the temperature of condensation.

The model has originally been compared to experimental results⁵⁹ on the kinetic energy distributions of neutral atoms sputtered from condensed rare gases under Ar⁺, Xe⁺, and Kr⁺ ion bombardment.¹⁹ It was demonstrated that the shape of the energy distribution—including its maximum at very low energies—could be correctly reproduced. Here, we fit the

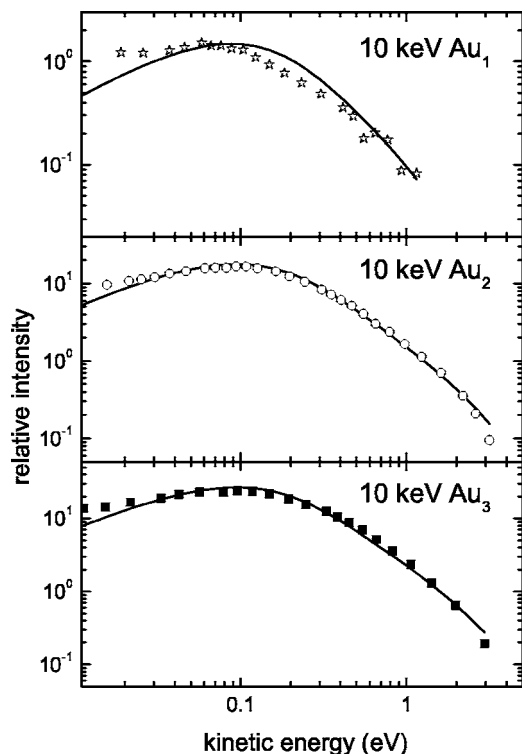


FIG. 8. Spike contribution of kinetic emission energy spectra of neutral In atoms sputtered from a polycrystalline indium surface under impact of 10-keV Au_m^- projectiles. Solid lines: least-squares fit of Urbassek-Michl (Ref. 19) gas flow model.

prediction of Eq. (4) to the data presented in Fig. 6, using the initial spike core temperature T_0 and the recondensation temperature T_{con} as adjustable parameters. The results are shown in Fig. 8. It is clearly seen that our experimental data are in much better agreement with the prediction from the gas flow model in comparison with the thermal spike model. In the case of diatomic and triatomic projectiles, the best fit is found for $T_0=18\,000$ K and $T_{con}=700$ K. For monoatomic projectiles, the parameters are determined as 9000 K and 650 K, respectively. As outlined in Ref. 19, the initial spike core temperature may be estimated theoretically from the (nuclear) stopping power S of the solid for the projectile as

$$T_0 = \frac{S}{\pi C \rho_{\perp}^2} \quad (6)$$

where $C=3/2nk$ is the heat capacity of the target material and ρ_{\perp} is the lateral width of the energized volume. For a rough estimate, we will take the density of indium ($n=38.3\text{ nm}^{-3}$) and $\rho_{\perp}\sim 3\text{ nm}$, which is about the mean dimension of the emission area obtained from molecular dynamics (MD) simulations,⁶⁰ and use the stopping power predicted from SRIM2003 calculations. At the impact energy of 10 keV, the calculated values of $S=203, 297,$ and $361\text{ eV}/\text{\AA}$ for $\text{Au}_1, \text{Au}_2,$ and Au_3 projectiles, respectively, result in $T_0=14\,600, 21\,400,$ and $26\,000\text{ K}$ in reasonably good agreement with the values extracted from the fits.

It should be noted that the magnitude of the initial spike core temperature T_0 calculated by Eq. (6) is in all cases

larger than the critical temperature of indium (6323 K). Similar values are obtained if the core temperature is estimated in the framework of the thermal spike theory.¹⁶ On the basis of this finding, an emission mechanism described as thermal evaporation from a flat, hot solid or liquid surface must clearly be ruled out. This fact was also realized by Oostra *et al.*,²⁰ who argued that the discrepancy between the high temperature values extracted from their experiment and a thermal evaporation mechanism might be caused by the very short time scale of the spike evolution. Going one step further, we note that the high energy density in the cascade volume leads to a fundamentally different situation where the criteria for the applicability of phase explosion dynamics described, e.g., by the gas flow model appear to be fulfilled. There are, however, still a few details where our results deviate from the prediction of the theoretical model. For instance, the parameter T_{con} was originally estimated as the boiling temperature of the target material.¹⁹ In our fit, this parameter is determined to be significantly lower, i.e., somewhere between the boiling and melting temperatures of indium (2345 K and 430 K, respectively). The reason behind that discrepancy is unclear at the present time. It should be kept in mind, however, that the model was originally developed to describe the sputtering process of frozen noble gases. These materials exhibit extremely low sublimation energies, critical temperatures, etc., and, therefore, are very much different from the target material studied here. Although the resemblance between both spike emission mechanisms appears to be remarkable, we stress that it is by no means clear whether the underlying physics can simply be scaled from frozen noble gases toward metallic targets.

The gas flow model in its published form does not make any prediction regarding the emission energy distribution of sputtered clusters. This situation is unfortunate, since the remarkable similarity of monomer and dimer velocity distributions visible in Fig. 7 seems to represent a characteristic feature of the spike emission mechanism. In order to examine the underlying dynamics in a little more detail, we present results of MD computer simulations performed for self-sputtering of silver surfaces under impact of small silver clusters.^{60,61} As an example, Fig. 9 shows temporal snapshots of the collision cascade developing under impact of a 6-keV Ag_3 projectile onto an $\text{Ag}(111)$ surface. For details regarding this calculation, the reader is referred to our original publication.⁶⁰ In order to reveal more insight, the crystal of $140\times 140\times 70\text{ \AA}^3$ dimension is cut such that only atoms located in a central slab of 14 \AA thickness are visible. The presented trajectory represents a case leading to large action, resulting in a total sputter yield of about 70 atoms. The surface disruption and crater formation, which have also been observed experimentally²⁶ and, therefore, seem to be typical for spikes, are clearly visible. In fact, these dynamics closely resemble those calculated by Postawa *et al.* for impact of a 20-keV C_{60} cluster onto the same silver surface.^{62,63} Close inspection reveals that during the later stage of the cascade, all particles within the crater area—atoms and clusters—tend to move collectively away from the surface with similar velocities. These collective dynamics agree with our experimental findings and appear to be typical for the particle emission mechanism induced by a collisional spike.

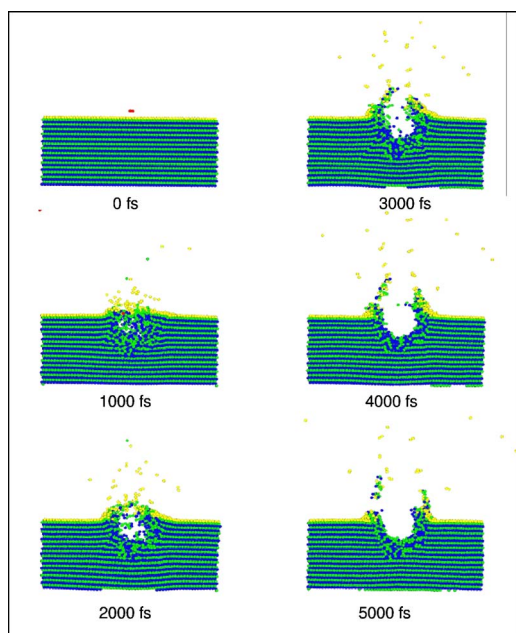


FIG. 9. (Color online) Temporal snapshots of a MD simulation performed for normal incidence of a 6-keV Ag₃ projectile onto an Ag(111) surface. Only the central slab of the crystal with a thickness of 1.4 nm is shown for clarity

IV. CONCLUSION

The yields and energy distributions of neutral particles sputtered from a metal surface under bombardment with heavy gold cluster projectiles present clear evidence for the formation of collisional spikes. Our results show the relative importance of a spike-induced emission mechanism to strongly grow with increasing nuclearity and energy of the projectile. While bombardment of indium with 5-keV Au₁ still leads to observables which are in excellent agreement with the prediction of linear cascade sputtering theory, the

impact of 10-keV Au₂ or Au₃ apparently generates completely spike-dominated dynamics. However, it is also evident that the particle emission mechanism prevailing under these conditions cannot be interpreted in terms of thermal evaporation from a locally heated solid. This finding is easily rationalized by the fact that spike temperatures producing the observed nonlinear yield enhancement would necessarily have to be of the order of 10⁴ K, i.e., larger than the critical temperature of the developing material. Therefore, the material in the core of the developing collision cascade is rapidly transformed into a gas-phase state, leading to a phase explosion of the overheated and, hence, strongly pressurized cascade volume. MD simulations reveal that the surface is completely disrupted in such a process, followed by a quasifree expansion of the material into the vacuum. In fact, our experimental data are found to agree quite well with a “gas flow” model designed to describe such a scenario. In particular, the model explains the experimental observation of most probable emission energies to be much lower than both the “thermal” energy in the cascade volume and the sublimation energy of the target material. The gas expansion scenario is corroborated even more by the fact that under spike conditions the emission velocity distributions of sputtered monomers and clusters are found to be practically identical. This result, which would be highly untypical for linear cascade sputtering, appears to be another key feature of collisional spikes developing under polyatomic ion bombardment of metal targets.

ACKNOWLEDGMENTS

The authors wish to thank the German Science Foundation (Deutsche Forschungsgemeinschaft) for financial support in the frame of the Sonderforschungsbereich 616 entitled “Energy Dissipation at Surfaces.” One of us (A.S.) would also like to thank the Graduiertenkolleg “Reactivity near Surfaces” for financial support.

¹For a review see *Sputtering by Particle Bombardment*, edited by R. Behrisch *et al.* (Springer, Berlin, 1981, 1983, and 1991), Vols. I–III.

²P. Sigmund, *Phys. Rev.* **184**, 383 (1969).

³P. Sigmund, in *Sputtering by Particle Bombardment I*, edited by R. Behrisch (Springer, Berlin, 1981), Vol. 1, p. 9.

⁴M. W. Thompson, *Philos. Mag.* **18**, 377 (1968).

⁵W. O. Hofer, in *Sputtering by Particle Bombardment III*, edited by R. Behrisch and K. Wittmaack (Springer, Berlin, 1991), Vol. 3, p. 15.

⁶W. Eckstein, *Computer Simulation of Ion-Solid Interactions* (Springer, Berlin, 1991).

⁷H. H. Andersen, in *Fundamental Processes in Sputtering of Atoms and Molecules (SPUT 92)*, edited by P. Sigmund (Det Kongelige Danske Videnskabernes Selskab, Copenhagen, 1993), p. 127.

⁸H. H. Andersen and H. L. Bay, *J. Appl. Phys.* **45**, 953 (1974).

⁹D. A. Thompson and S. S. Johar, *Radiat. Eff.* **55**, 91 (1981).

¹⁰D. A. Thompson and S. S. Johar, *Nucl. Instrum. Methods* **170**, 281 (1980).

¹¹S. S. Johar and D. A. Thompson, *Surf. Sci.* **90**, 319 (1979).

¹²D. A. Thompson and S. S. Johar, *Appl. Phys. Lett.* **34**, 342 (1979).

¹³S. Bouneau, A. Brunelle, S. Della-Negra, J. Depauw, D. Jacquet, Y. Le Beyec, M. Pautrat, M. Fallavier, J. C. Poizat, and H. H. Andersen, *Phys. Rev. B* **65**, 144106 (2002).

¹⁴H. H. Andersen, A. Brunelle, S. Della-Negra, J. Depauw, D. Jacquet, Y. Le Beyec, J. Chaumont, and H. Bernas, *Phys. Rev. Lett.* **80**, 5433 (1998).

¹⁵P. Sigmund, *Nucl. Instrum. Methods Phys. Res. B* **164**, 401 (2000).

¹⁶P. Sigmund and C. Claussen, *J. Appl. Phys.* **52**, 990 (1981).

¹⁷P. Sigmund, *Appl. Phys. Lett.* **25**, 169 (1974).

¹⁸R. Kelly, *Radiat. Eff.* **80**, 273 (1984).

¹⁹H. M. Urbassek and J. Michl, *Nucl. Instrum. Methods Phys. Res. B* **22**, 480 (1987).

- ²⁰D. J. Oostra, R. P. van Ingen, A. Haring, A. E. de Vries, and F. W. Saris, *Phys. Rev. Lett.* **61**, 1392 (1988).
- ²¹L. Wang, N. R. Md, and W. G. Graham, *J. Phys. D* **30**, 2379 (1997).
- ²²S. Ghalab and A. Wucher, *Nucl. Instrum. Methods Phys. Res. B* **226**, 264 (2004).
- ²³A. V. Samartsev and A. Wucher (unpublished).
- ²⁴M. Wahl and A. Wucher, *Nucl. Instrum. Methods Phys. Res. B* **94**, 36 (1994).
- ²⁵C. Staudt and A. Wucher, *Phys. Rev. B* **66**, 075419 (2002).
- ²⁶R. C. Birtcher, S. E. Donnelly, and S. Schlutig, *Nucl. Instrum. Methods Phys. Res. B* **215**, 69 (2004).
- ²⁷L. E. Rehn, R. C. Birtcher, P. M. Baldo, A. W. McCormick, and L. Funk, *Nucl. Instrum. Methods Phys. Res. B* **212**, 326 (2003).
- ²⁸L. E. Rehn, R. C. Birtcher, S. E. Donnelly, P. M. Baldo, and L. Funk, *Phys. Rev. Lett.* **87**, 207601-1 (2001).
- ²⁹For information on the SRIM2003 Monte-Carlo simulation program see *The Stopping and Range of Ions in Solids*, edited by J. F. Ziegler, J. P. Biersack, and U. Littmark, 2nd ed. (Pergamon Press, New York, 2003). See also <http://www.srim.org>
- ³⁰N. Matsunami, Y. Yamamura, Y. Itikawa, N. Itoh, Y. Kazumata, S. Miyagawa, K. Morita, R. Shimizu, and H. Tawara, *At. Data Nucl. Data Tables* **31**, 1 (1984).
- ³¹D. A. Thompson, *Radiat. Eff.* **56**, 105 (1981).
- ³²M. W. Thompson, *Phys. Rep.* **69**, 335 (1981).
- ³³H. H. Andersen and H. L. Bay, in *Sputtering by Particle Bombardment I*, edited by R. Behrisch (Springer, Berlin, 1981), Vol. 1, p. 145.
- ³⁴A. Wucher, M. Wahl, and H. Oechsner, *Nucl. Instrum. Methods Phys. Res. B* **82**, 337 (1993).
- ³⁵M. W. Thompson and R. S. Nelson, *Philos. Mag.* **45**, 2015 (1962).
- ³⁶M. Szymonski and A. Poradzisz, *Appl. Phys. A* **28**, 175 (1982).
- ³⁷M. Szymonski, R. S. Bhattacharya, H. Overeijnder, and A. E. de Vries, *J. Phys. D* **11**, 751 (1978).
- ³⁸M. Szymonski and A. E. de Vries, *Phys. Lett.* **63A**, 359 (1977).
- ³⁹H. Overeijnder, M. Szymonski, A. Haring, and A. E. de Vries, *Phys. Status Solidi B* **81**, K11 (1977).
- ⁴⁰C. Staudt and A. Wucher (unpublished).
- ⁴¹S. R. Coon, W. F. Calaway, M. J. Pellin, J. W. Burnett, and J. M. White, *Surf. Interface Anal.* **20**, 1007 (1993).
- ⁴²F. Bernhardt, H. Oechsner, and E. Stumpe, *Nucl. Instrum. Methods* **132**, 329 (1976).
- ⁴³R. A. Brizzolara and C. B. Cooper, *Nucl. Instrum. Methods Phys. Res. B* **43**, 136 (1989).
- ⁴⁴S. R. Coon, W. F. Calaway, M. J. Pellin, G. A. Curlee, and J. M. White, *Nucl. Instrum. Methods Phys. Res. B* **82**, 329 (1993).
- ⁴⁵S. R. Coon, W. F. Calaway, J. W. Burnett, M. J. Pellin, D. M. Gruen, D. R. Spiegel, and J. M. White, *Surf. Sci.* **259**, 275 (1991).
- ⁴⁶Z. Ma, W. F. Calaway, M. J. Pellin, and E. I. Nagy-Felsobuki, *Nucl. Instrum. Methods Phys. Res. B* **94**, 197 (1994).
- ⁴⁷W. Gerhard, *Z. Phys. B* **22**, 31 (1975).
- ⁴⁸H. Oechsner, in *The Physics of Ionized Gases*, edited by M. M. Popovic and P. Krstic (World Scientific Publishing Co. Pte Ltd., Singapore, 1985), p. 571.
- ⁴⁹G. P. Koennen, A. Tip, and A. E. de Vries, *Radiat. Eff.* **21**, 269 (1974).
- ⁵⁰C. T. Reimann, in *Fundamental Processes in Sputtering of Atoms and Molecules (SPUT 92)*, edited by P. Sigmund (Det Kongelige Danske Videnskabernes Selskab, Copenhagen, 1993), p. 351.
- ⁵¹H. Haberland, in *Clusters of Atoms and Molecules, Theory, Experiment, and Clusters of Atoms*, edited by H. Haberland (Springer, Berlin, 1994), p. 207.
- ⁵²H. M. Urbassek and K. T. Waldeer, *Phys. Rev. Lett.* **67**, 105 (1991).
- ⁵³K. T. Waldeer and H. M. Urbassek, *Nucl. Instrum. Methods Phys. Res. B* **73**, 14 (1993).
- ⁵⁴R. S. Averback and M. Ghaly, *Nucl. Instrum. Methods Phys. Res. B* **127–128**, 1 (1997).
- ⁵⁵E. M. Bringa, R. E. Johnson, and L. Dutkiewicz, *Nucl. Instrum. Methods Phys. Res. B* **152**, 267 (1999).
- ⁵⁶E. M. Bringa, M. M. Jakas, and R. E. Johnson, *Nucl. Instrum. Methods Phys. Res. B* **164–165**, 762 (2000).
- ⁵⁷M. M. Jakas, E. M. Bringa, and R. E. Johnson, *Phys. Rev. B* **65**, 165425 (2002).
- ⁵⁸H. H. Andersen, A. Johansen, and V. S. Touboltsev, *Nucl. Instrum. Methods Phys. Res. B* **164–165**, 727 (2000).
- ⁵⁹R. A. Haring, R. Pedrys, A. Haring, and A. E. de Vries, *Nucl. Instrum. Methods Phys. Res. B* **232**, 40 (1984).
- ⁶⁰M. Lindenblatt, R. Heinrich, A. Wucher, and B. J. Garrison, *J. Chem. Phys.* **115**, 8643 (2001).
- ⁶¹A. Duvenbeck, M. Lindenblatt, and A. Wucher, *Nucl. Instrum. Methods Phys. Res. B* **228**, 170 (2005).
- ⁶²Z. Postawa, B. Czerwinski, M. Szewczyk, E. J. Smiley, N. Winograd, and B. J. Garrison, *Anal. Chem.* **75**, 4402 (2003).
- ⁶³Z. Postawa, B. Czerwinski, M. Szewczyk, E. J. Smiley, N. Winograd, and B. J. Garrison, *J. Phys. Chem. B* **108**, 7831 (2004).